Fachtagung "Experimentelle Strömungsmechanik"
5. – 7. September 2017, Karlsruhe

Reduzierter Bewertungsfehler bei der Kreuzkorrelation Brechungsindex angepasster und oberflächenbeschichteter Suspensionspartikel

Reduced Estimation Error of Cross-Correlation Based Displacements of Refractive Index Matched and Surface Labelled Suspension Particles

Sebastian Blahout, Jeanette Hussong
AG Lasermesstechnik der Mehrphasenströmungen,
Lehrstuhl für Hydraulische Strömungsmaschinen,
Ruhr-Universität Bochum, Universitätsstr. 150, 44801 Bochum

µPIV, Suspensionsströmung, Brechungsindexanpassung
µPIV, Suspension Flow, Refractive Index Matching

Abstract

In the present study, we report on reduced particle image size sensitivity for µPIV evaluations of suspension flows through fluorescence surface labelling. Due to refractive index matching, particles assume M-shaped intensity profiles which leads to a reduced estimation error for PIV evaluations in comparison to particles of Gaussian intensity profile.
Exemplary µPIV results on M-shaped suspension particle images in a microchannel with 5 Vol-% particle volume fraction are presented.

Introduction

While bulk properties of dense suspensions are well describable, more complex flow dynamics of suspensions with inhomogeneous microstructural properties are still little understood and have gained increasing interest throughout the last decades [Krieger 1972, Ackerson 1990, Guazzelli et al. 2012]. Recent investigations showed for example, that a near wall particle depletion region evolves within the viscous sublayer of turbulent, monodisperse and neutrally buoyant suspension flows due to hydrodynamic particle interactions, leading to a wall-shear increasing behaviour [Costa et al. 2017]. Also sheared suspensions beyond 30% volume fraction may be affected by microstructural dynamics such as hydroclustering or particle banding [Morris 2009].
While detailed numerical studies of monodisperse, dense suspension flows with microstructural finite-size particle interactions are advancing fast, corresponding optical investigations are still rare [Maxey 2017, Denn and Morris 2014].
Especially a limited optical accessibility of dense suspension flows makes the application of non-invasive measurement methods difficult. However, in liquid flows suspension components of matched refractive indices may be used to minimize light scattering at particle fluid interfaces, resulting in transparent suspension particles.
As the packing density of suspension flows easily exceeds $\mathcal{O}(10^{-2})$ particles per pixels (i.e. approximately 65 pixels particle image diameter, 5 Vol-% packing density and a correlation depth that equals the particle image diameter), PIV is the preferred choice to access particle

Karlsruhe, Germany, ISBN 978-3-9816764-3-3

displacement fields [Wereley and Meinhart 2010]. In regions where microstructural changes of the suspension flow leads to observable differences in particle image displacements over a length scale comparable to the interrogation window size, super-resolution PIV may be applied [Keane et al. 1995]. In microfluidic applications, such situations may be encountered close to interfaces or locally confined regions of high or even discontinuous shearing planes [Morris 2009]. Since the particle size itself is not a free experimental parameter, in suspension flow studies, it may be one or two orders larger than for tracer particles usually used in µPIV.
In the present study, we report on a reduced particle image size sensitivity for µPIV evaluations of suspension flows through fluorescence surface labelling. Due to refractive index matching, these particles obtain an M-shaped, instead of a Gaussian intensity profile as it is known from classical PIV particle images. It is this M-shaped intensity profile that ensures a reduced estimation error at large image diameters. Thus, in the present study advantages of a high optical accessibility and reduced characteristic particle image size are combined through refractive index matching and fluorescence labelling.
In this paper, differences between the detectability and the estimation error of M-shaped and Gaussian particles are discussed and µPIV results of a suspension of M-shaped particle images are presented in a microchannel flow with 5 Vol-% particle volume fraction.

Theoretical Background

For the evaluation of PIV cross-correlation results the correlation peak detectability and the estimation error are essential. Both are calculated from the cross-correlation result. In this paper, the cross-correlation of double-framed, single-exposure images is considered, solely. The correlation value of the highest correlation peak is called R_D. Its location indicates the displacement of a particle image group within the corresponding interrogation window between the first and second frame [Keane and Adrian 1992].

Correlation Peak Detectability

The correlation peak detectability is defined as the ratio between the highest and the second highest correlation peak value [Coupland and Pickering 1988, Keane and Adrian 1990]. Physically, the detectability can be interpreted as the probability at which the displacement correlation peak R_D, is correctly identified as valid [Adrian and Westerweel 2011].

Estimation Error

It was shown by Willert and Gharib, that the absolute measurement error of a PIV measurement can be reduced by using a proper peak fit estimator [Willert and Gharib 1991]. By this, the correlation peak location can be estimated to a sub-pixel order, while reducing peak locking effects [Westerweel 1997]. Since the shape of the displacement correlation peak is usually approximately Gaussian, a Gaussian peak fit estimator $\hat{\epsilon}_G$ may be defined as follows [Westerweel 1997]:

$$\hat{\epsilon}_G = \frac{\ln(R^*_{-1}) - \ln(R^*_{+1})}{2\,[\ln(R^*_{-1}) + \ln(R^*_{+1}) - 2\ln(R^*_0)]} \quad \textbf{(1)}$$

Here R^*_0 equals R_D and $R^*_{\pm 1}$ are the correlation values next to R^*_0 in positive and negative axis direction, respectively. The variance of the Gaussian peak fit estimator represents the error of the estimated fractional displacement. It is usually referred to as estimation error and can be defined as [Westerweel 1997]:

Karlsruhe, Germany, ISBN 978-3-9816764-3-3

$$var(\hat{\epsilon}_G) \approx \sum_{i=-1}^{+1} \sum_{j=-1}^{+1} \frac{\partial \hat{\epsilon}_G}{\partial R_i^*} \frac{\partial \hat{\epsilon}_G}{\partial R_j^*} cov\{R_i^*, R_j^*\} \quad \textbf{(2)}$$

For the simplest case of a zero displacement, equation (2) simplifies to:

$$var(\hat{\epsilon}_G) \approx \left(\frac{\partial \hat{\epsilon}_G}{\partial R_{\pm 1}^*}\right)^2 [var\{R_{-1}^*\} + var\{R_{+1}^*\} - 2cov\{R_{-1}^*, R_{+1}^*\}] \quad \textbf{(3)}$$

It was shown that the estimation error minimises at a particle image diameter of slightly more than two pixels.

At smaller particle image diameters, bias errors are dominating, thus the estimation error increases. At particle image diameters larger than two pixels, the estimation error increases due to random errors, which are proportional to the particle image diameter [Westerweel 1997, Willert 1996].

While the apparent particle image diameter scales with the actual particle size of Gaussian intensity distributions, it is only weakly related to the actual particle size for M-shaped intensity distributions. We show that this leads to a reduced displacement correlation peak width for large particle image diameters.

Experimental Setup and Measurement Procedure

Before the measurement, Polymethylmethacrylate (PMMA) beads are submerged into a solution of distilled water and a Rhodamine B dye. Hence, the particles are filtered from the water solution, dried and added to a refractive index matched carrier liquid consisting of a ternary mixture of ammonium thiocyanate (NH_4SCN), glycerine and water with a final refractive index of $n_D = 1.4762$ at the sodium D line and a theoretical density of 1.19 g/cm³, to match both the refractive index and the density of the suspended PMMA beads [Bailey and Yoda 2003, Lyon and Leal 1998]. A representative snapshot of the suspension can be seen in Fig. 2a.

µPIV measurements are performed in a suspension flow of 5% volume fraction PMMA beads of D_P = 60 µm diameter. With a rectangular channel of 300 µm height and 5 mm width the Reynolds number assumes Re = 5. A double pulsed Nd:YAG laser (70 mJ, Evergreen) was coupled into an upright microscope (Nikon Eclipse LV100) and particle images are recorded with a dual frame CCD camera (LaVision Imager SX 5M) at 5 Hz and 1000 µs interframing time. Particle images are taken at nine measurement planes of Δz = 15 µm equidistant spacing starting at the bottom of the channel. For each plane a set of 500 images are recorded.

Synthetic Image Data Generation

Synthetic particle images are created based on test measurements of refractive index matched, surface labelled suspension particles. For this, radial intensity distributions are extracted from more than 100 recorded particle images to gain a representative intensity distribution for the synthetic particle image generation. Synthetic images of Gaussian particle images are created for comparison. Five particle images are placed in a 256 x 256 pixels interrogation window. Recorded and synthetic images of PMMA particles are shown in Fig. 1. A noise level of 20% of the maximum particle image intensity was chosen in Figs. 1c) and d).

For subsequent investigations, the particle image diameter is varied from 1.6 up to 60 pixels for both types of particles. The outer particle image diameter is taken to be at the location where the particle image intensity assumes 10% of its maximum intensity value. Lower thresholds are tested to induce only a minor shift of the results without significant impact on the findings presented here.

Particle image positions are distributed randomly within the interrogation window and are varied for every particle image diameter to prevent systematic errors.

Karlsruhe, Germany, ISBN 978-3-9816764-3-3

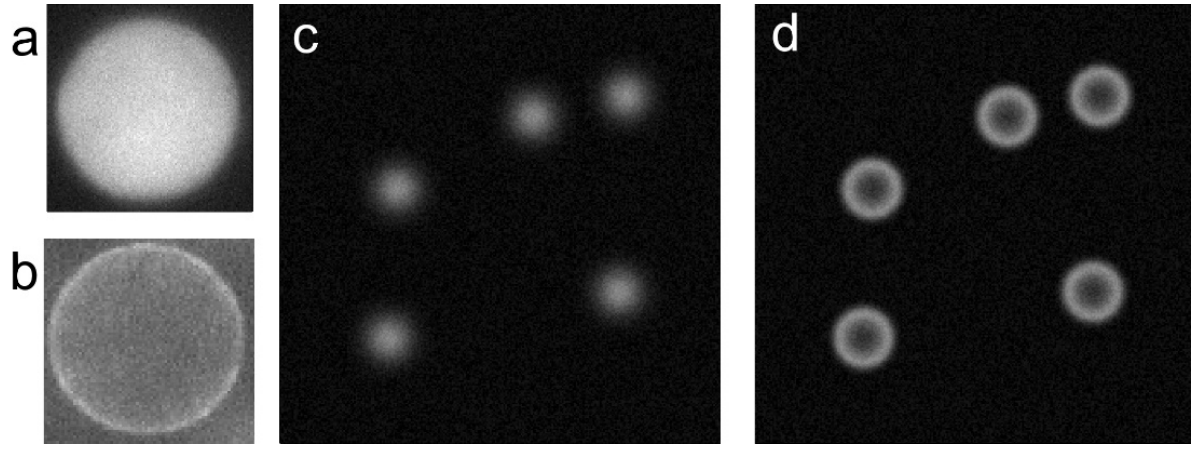

Fig. 1: a) Recorded particle image of a standard fluorescent microparticle (D_p = 60 µm); b) Recorded particle image of a refractive index matched fluorescent microparticle (D_p = 60 µm); c) Synthetic image of standard fluorescent microparticles (D_p = 40 pixels); d) Synthetic image of refractive index matched M-shaped particles (D_p = 40 pixels).

On the other hand, the same particle image locations are chosen for each particle image diameter when M-shaped and Gaussian particles are compared. For first investigations, an overlap of particles is suppressed, as well as particles cutting interrogation window edges. The influence of a particle overlap and in-plane losses on the estimation error and detectability will be investigated in the future.
Results without and with 20% noise level will be compared. To apply equation (3), a displacement vector between two cross-correlated frames of v_D = [0, 0] is chosen. Synthetic images are generated in Matlab and are processed in DaVis 8.4.0 (LaVision GmbH).

Experimental Data Evaluation

To improve the signal to noise ratio, a sliding average filter with a Gaussian weighting function of 2 pixels filter length is applied. Afterwards the sliding minimum over time is subtracted from the recorded image set to reduce background noise as shown in Fig. 2b). Due to the pre-processing procedure, the signal to noise ratio can be increased from approximately 1.2 in the raw image to a signal to noise ration of approximately 3. The PIV evaluation is performed using a final interrogation window size of 128 x 128 pixels. With an interrogation window overlap of 50% and a magnification of M = 3.5 this results in a vector spacing of approximately 60 µm.

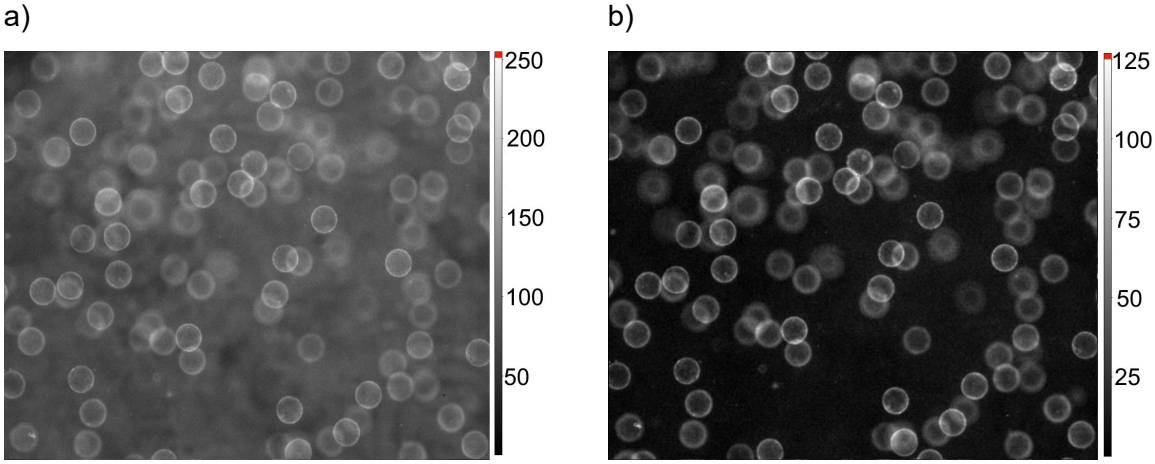

Fig. 2: a) Recorded raw image at z/D_P = 2 from the channel bottom; b) Pre-processing result of a).

Results

Optical Accessibility of the suspension flow

A refractive index matching of the suspension liquid to the particles is applied to 99.25% accuracy at 293 K. An ad-hoc test was done to access the quality of refractive index matching. This was done by traversing through a resting test volume of suspension with sedimented particles. The spacing between each traversing step corresponds to the particle diameter of D_P = 60 µm. An image series of six out of plane positions is shown in Fig. 5a)-f). Marked areas correspond to particles located in the respective focal plane. Thus, a sufficient optical accessibility could be realised to achieve an almost distortion-free view to six particle layers.

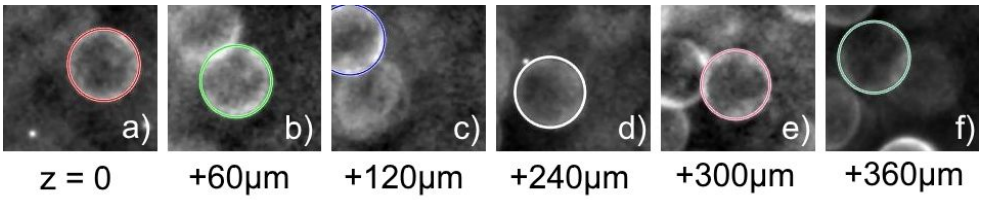

Fig. 3: Excerpts of overlapping refractive index matched suspension particles for the investigation of optical accessibility (Magnification M = 3.5, focal depth is 12.22 µm); a)-f): focal planes of 60 µm equidistant spacing scanning through five particle layers.

Particle Image and Correlation Peak Profiles

Estimation error and detectability are directly affected by the shape of the displacement correlation peak. The influence of the one-dimensional radial particle image intensity distribution on the shape of the displacement correlation peak of M-shaped and Gaussian particle images is displayed in Fig. 4.

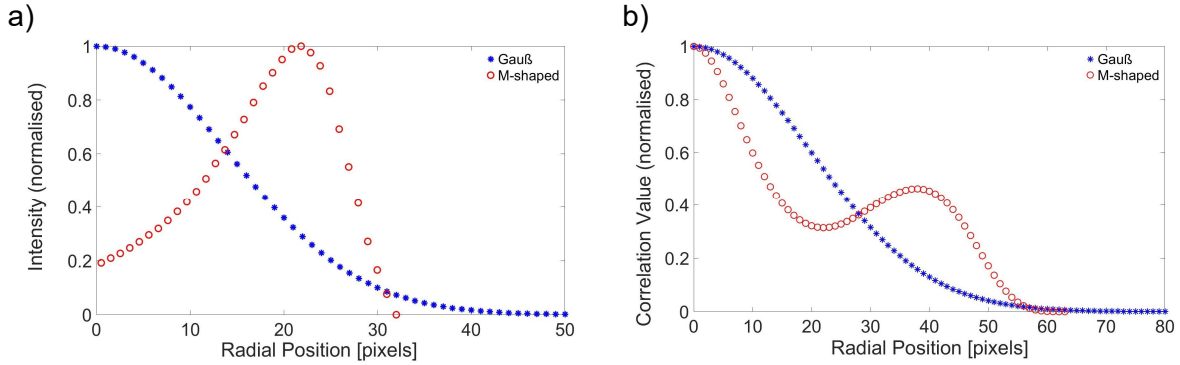

Fig. 4: a) One-dimensional radial intensity distribution of Gaussian and M-shaped particle images of D_P = 60 pixels; b) Resulting one-dimensional correlation function for a zero-displacement of a Gaussian and M-shaped particle image.

As mentioned earlier, the particle image diameter is defined through 10% of the maximum particle image intensity value. Fig. 4b) displays the resulting correlation peaks for a zero-displacement. As can be seen, the M-shaped particle image results in a narrower displacement correlation peak compared to that resulting from Gaussian particle images, but it likewise assumes a secondary correlation peak. This secondary peak is a result of the shape of the corresponding intensity distribution. It emanates from the correlation of a half particle image diameter displacement. It may be noted that the secondary peak shown here for a one-dimensional intensity profile is overestimated compared to those resulting from a full particle image (see Fig. 5b). That is because the actual particle image is rotationally symmetric, such that the

cross-correlation of two images results in a correlation peak, that is surrounded by a secondary, plateau-like peak region as shown in Fig. 5b).

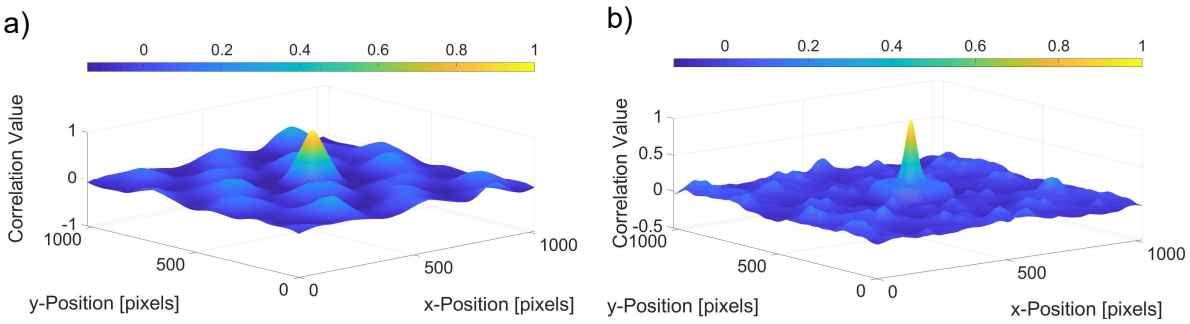

Fig. 5: Normalised correlation map gained from synthetic data for particle images with a particle image diameter of D_P = 140 pixels and a displacement vector of v_D = [50, 50] pixels (N_I = 5, Interrogation window size = Image size = 1024 x 1024 pixels); a) Gaussian particles; b) M-shaped particles.

Correlation Peak Detectability

The correlation peak detectability between synthetic data of M-shaped and Gaussian particle images is compared. Despite differences evident in the correlation map as shown in Fig. 5, the detectability of the displacement correlation peak R_D of both particle types averaged over an image diameter range of 1.6 – 60 pixels, assumes very similar values for both, particle images without and with 20% noise level (see Table 1).

Particle Image:	**Without noise:**	**20% noise level**
Gaussian	4.32 ± 1.18	4.00 ± 1.18
M-shaped	4.49 ± 1.06	4.29 ± 1.08

Table 1: Mean values for the correlation peak detectability of Gaussian and M-shaped particle images averaged for an image diameter range of 1,6-60 pixels.

We assume that the large standard deviations arise from varying, random particle distributions within the interrogation window. Further investigations are currently carried out on the influence of particle image density on the correlation peak detectability. Here, it is expected that the correlation peak detectability of M-shaped particle images will increasingly outperform those of a Gaussian intensity profile for a rising particle image density. This is expected as the probability of secondary correlation peaks emanating from false displacement detections rises.

Estimation Error

Fig. 6 shows the estimation error according to equation (3) in a semi-logarithmic scale without and with 20% noise level, respectively. As expected, for Gaussian particle images, a minimum estimation error occurs at approximately two pixels particle image diameter, while for larger particle images the estimation error increases.
From Fig. 6a) it is evident, that the estimation error from M-shaped particle images is lower than for Gaussian particle images. That is because the apparent particle image diameter for Gaussian particles scales with the actual particle size while the relevant length scale of M-shaped particle images is directly related to the width of the fluorescent signal at the particle rim. First tests showed that the relevant reference length of M-shaped particles corresponds to the width of the particle image rim at an intensity level of approximately 50% with respect to the maximum particle image intensity.

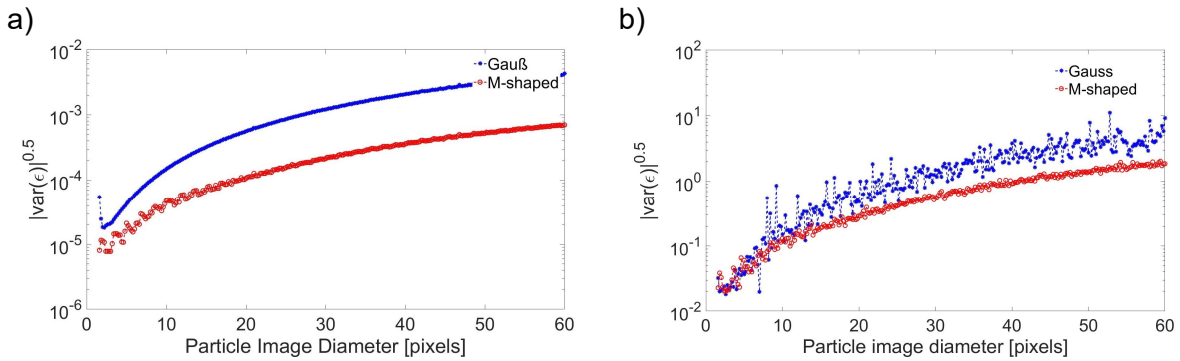

Fig. 6: Estimation error of M-shaped and Gaussian particles a) without noise; b) with noise.

As shown in Fig. 6b) the presence of noise leads to a significant increase of the estimation error for both particle types. It may be noted, that due to experimental observations (see Fig. 1), the influence of a random noise level of 20% over the whole field of view is investigated here rather than background noise. We assume that the increase in the estimation error originates from an stronger decorrelation of particle images, leading to a flattening of the correlation peak, which in turn leads to an increase of the peak fit estimator derivative (first term in equation (3)).

Experimental Measurements

A test measurement of a microchannel flow with 5% particle volume fraction is performed, as described previously. Resulting vector fields of four measurement planes at 30 µm, 60 µm, 90 µm and 120 µm spacing to the bottom wall are shown in Fig. 7.

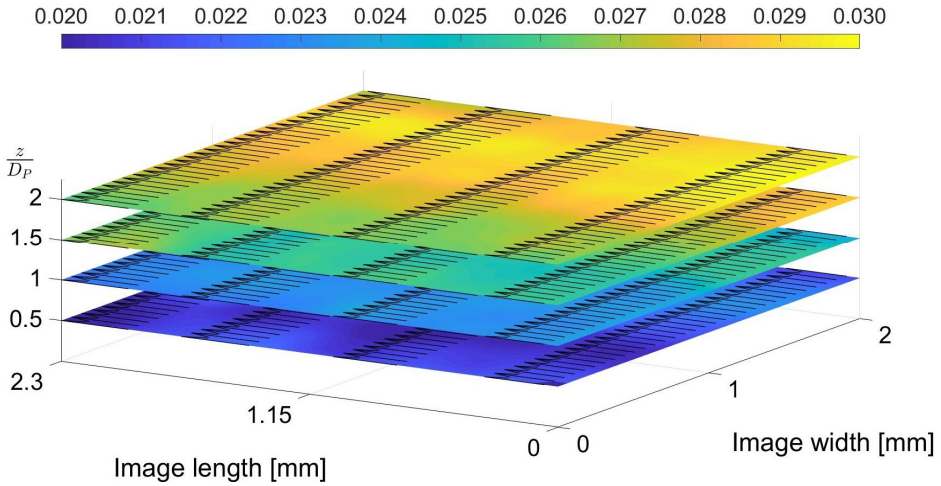

Fig. 7: Velocity vector fields at different z-positions from the channel bottom divided by the particle diameter for D_P = 60 µm PMMA M-shaped particles at a Reynolds number of Re = 5.

An ensemble of 500 images was taken for each measurement plane. The shown vector fields contain less than 1% outliers (outliers were defined as correlations with detectability below 1.1). In-plane velocity gradients are visible in the vector field results. These are no artefacts from the PIV evaluation itself, but are a characteristic of the investigated suspension flow. From numerical simulations, it was found that in square duct microchannel flows neutrally buoyant suspension particles of 5 Vol-% and a channel height to particle diameter ratio of 9 tend to assume significant variations in particle velocities U_P compared to fluid velocities U_f with a maximum p.d.f. for U_P/U_f of 0.5 [Kazerooni et al. 2017]. Future measurements aim to confirm these trends experimentally.

Conclusions & Outlook

µPIV measurements have been successfully applied to a refractive index matched suspension of surface labelled and refractive index matched PMMA particles. It could be shown that those particles assume an M-shaped, radial intensity distribution, which reduces the estimation error in comparison to Gaussian particle images of the same particle image size.
From synthetic image data, it is evident that the estimation error of M-shaped particle images reduces for both, images without and with 20% noise level, respectively. It was shown, that for M-shaped particle images, the characteristic particle image length scales with the fluorescent intensity peak at the particle rim instead of the actual particle image diameter.
To provide a more complete picture of the applicability of refractive index matched and surface labelled suspension particles for µPIV measurements, future studies aim to reveal their influence on the focal depth, out-of-plane and in-plane losses for different particle concentrations.

Literature

Krieger, I.M., 1972: "Rheology of Monodisperse Latices", Advances in Colloid and Interface Science 3, Nr. 2: 111–36.
Ackerson, B.J., 1990: "Shear Induced Order and Shear Processing of Model Hard Sphere Suspensions", Journal of Rheology 34, Nr. 4: 553–90.
Guazzelli, E., Morris, J.F., Pic, S., 2012: "A physical introduction to suspension dynamics", Cambridge texts in applied mathematics (Cambridge; New York: Cambridge University Press).
Costa, P., Picano, F., Brandt, L., Breugem, W.P., 2017: "Finite size effects in dense turbulent wall-bounded transport of neutrally-buoyant spheres", arXiv preprint arXiv:1703.06036.
Morris, J.F., 2009: "A Review of Microstructure in Concentrated Suspensions and Its Implications for Rheology and Bulk Flow", Rheologica Acta 48, Nr. 8: 909–23.
Maxey, M., 2017: "Simulation Methods for Particulate Flows and Concentrated Suspensions", Annual Review of Fluid Mechanics 49, Nr. 1: 171–93.
Denn, M.M., Morris, J.F., 2014: "Rheology of Non-Brownian Suspensions", Annual Review of Chemical and Biomolecular Engineering 5, Nr. 1: 203–28.
Wereley, S.T., Meinhart, C.D., 2010: "Recent Advances in Micro-Particle Image Velocimetry", Annual Review of Fluid Mechanics 42, Nr. 1: 557–76.
Keane, R.D., Adrian, R.J., Zhang, Y., 1995: "Super-resolution particle imaging velocimetry", Measurement Science and Technology 6, Nr. 6: 754.
Keane, R.D., Adrian, R.J., 1992: "Theory of cross-correlation analysis of PIV images", Applied scientific research 49, Nr. 3 (1992): 191–215.
Coupland, J.M., Pickering, C.J.D., 1988: "Particle Image Velocimetry: Estimation of Measurement Confidence at Low Seeding Densities", Optics and Lasers in Engineering 9, Nr. 3–4: 201–10.
Keane, R.D., Adrian, R.J., 1990: "Optimization of particle image velocimeters. I. Double pulsed systems", Measurement Science and Technology 1, Nr. 11: 1202–15.
Adrian, R.J., Westerweel, J., 2011: "Particle Image Velocimetry", Cambridge Aerospace Series 30 (Cambridge; New York: Cambridge University Press).
Westerweel, J., 1997: "Fundamentals of digital particle image velocimetry", Measurement Science and Technology 8, Nr. 12: 1379.
Willert, C.E., Gharib, M., 1991: "Digital particle image velocimetry", Experiments in fluids 10, Nr. 4: 181–193.
Willert, C., 1996: "The fully digital evaluation of photographic PIV recordings", Applied Scientific Research 56, Nr. 2: 79–102.
Bailey, B.C., Yoda, M., 2003: "An aqueous low-viscosity density- and refractive index-matched suspension system", Experiments in Fluids 35, Nr. 1: 1–3.
Lyon, M.K., Leal, L.G., 1998: "An experimental study of the motion of concentrated suspensions in two-dimensional channel flow. Part 1. Monodisperse systems", Journal of Fluid Mechanics 363: 25–56.
Kazerooni, H.T., Fornari, W., Hussong, J., Brandt, L., 2017: "Inertial migration in dilute and semi-dilute suspensions of rigid particles in laminar square duct flow", arXiv preprint arXiv:1705.08734.